Supplementary Text: Mechanistic Investigation of APEX2

Here we discuss our additional efforts to understand why the A134P mutation in APEX2 renders it far more active than APEX inside cells. In the main text, we described how the most striking difference we could detect between APEX and APEX2 was their varying susceptibilities to H_2O_2-induced inhibition. In the presence of 1.4 mM of the model phenolic substrate guaiacol, APEX displayed severe inhibition at >250 μM H_2O_2. This is consistent with the previous finding that wild-type pea APX is very sensitive to H_2O_2 inhibition.[1] On the other hand, APEX2 initial rates continued to climb (i.e., APEX2 was resistant to H_2O_2-induced inhibition) beyond 5 mM H_2O_2 (Figure 2E). Thus, in this assay, APEX2 resembled HRP more than it resembled APEX; HRP oxidation rates also climbed until the H_2O_2 concentration reached 10 mM. Furthermore, in this kinetic assay, APEX and dimeric ^{W41F}APX displayed nearly identical behavior, as did APEX2 and ^{VPG}APEX. These observations suggest that H_2O_2 sensitivity is independent of peroxidase oligomerization state, and is not affected by certain mutations remote from the active site.

Why does the A134P mutation in APEX2 cause it to be much more resistant to H_2O_2-induced inhibition? Both irreversible and reversible forms of H_2O_2 inhibition have been reported for peroxidases.[2,3] The former proceeds through covalent modification of heme. The latter involves trapping of the heme co-factor in a catalytically inactive state, Compound III (Supplementary Fig. 12). To determine the relevant mechanism of inhibition, we performed two inhibition reversibility tests. Supplementary Fig. 13 A-B shows that, on the yeast surface, pre-treatment of APEX or APEX2 with a burst of high H_2O_2 (10 mM for 1 minute) does not reduce its subsequent activity. On purified proteins (Supplementary Fig. 13C), we used elevated guaiacol concentrations to rescue the enzyme from a high H_2O_2 pretreatment step (10 mM for 1 minute). Again, both APEX and APEX2 activity fully recovered from the pretreatment, suggesting that the inhibition is of a reversible, rather than irreversible, nature.

How does APEX2 avoid reversible H_2O_2 inhibition better than APEX? If the inhibition proceeds through Compound III, the A134P mutation could either decelerate the reaction between Compound II and H_2O_2 to form Compound III, or it could accelerate the productive reaction between Compound II and guaiacol. Though we have not investigated this question in detail, we did measure the kinetic parameters for guaiacol oxidation by each peroxidase (Supplementary Fig. 14). Given the different H_2O_2 susceptibilities, we performed the measurements at the H_2O_2 concentration that was optimal (i.e., gave Michaelis-Menten behavior and avoided severe H_2O_2-induced inhibition) for each peroxidase: 90 μM for APEX and ^{W41F}APX; 1 mM for APEX2 and ^{VPG}APEX; and 10 mM for HRP. Our measurements showed that both k_{cat} and K_M (for guaiacol) were improved for APEX2 compared to APEX, leading to a catalytic efficiency enhancement of 2.95-fold.

In summary, our mechanistic experiments suggest a model in which the A134P mutation in APEX2 alters the conformation of the substrate binding loop to improve recognition and turnover of aromatic substrates. This results in a modest improvement to k_{cat} and K_M, but has a much more dramatic effect on the resistance of APEX2 to reversible H_2O_2-induced inhibition, perhaps by diverting Compound II back to the resting state and thereby minimizing the opportunity for trapping in the non-productive Compound III state. Interestingly, we found that proline at 134 is specifically required for this effect, since replacement with other sidechains (Ile, Val, Gly) resulted in much lower peroxidase activity at both low and high H_2O_2 concentrations (Supplementary Fig. 15).

After characterizing APEX2, we performed sequence alignments of all listed Class I, II, and III peroxidases available at Peroxibase (http://peroxibase.toulouse.inra.fr/index.php).[4] Intriguingly, the majority of sequenced Class II and III peroxidases, including HRP, already possess proline at the position corresponding to A134 in APEX (Supplementary Fig. 11). Class II and III peroxidases are secreted, disulfide-containing proteins, in contrast to the cytosolic Class I peroxidases from which APEX2 is derived. Of the 632 listed Class I ascorbate peroxidases, more than 75% have alanine at the position corresponding to 134, with only 22 possessing proline. Of those 22, three are likely mis-annotated Class III peroxidases (GsAPx06, GsAPx08, GsAPx05).[5] The segregation of amino acid identity at this position by peroxidase class, which was previously noted,[6] suggests that this proline may have an important functional role for Class II/III peroxidases. Apart from their existence in oxidizing environments that may have higher H_2O_2 concentrations, Class II/III peroxidases primarily utilize aromatic substrates,[7,8]

suggesting a specific role for proline in enhancing phenol oxidation. Indeed, when we mutated the analogous 141P in HRP to Ala, we observed a significant drop in activity towards biotin-phenol (Supplementary Fig. 15). It is striking that our directed evolution experiment converged upon the same solution obtained by natural evolution.

In the course of our kinetic experiments, we noticed that both APEX and APEX2 were susceptible to an additional mechanism of inhibition on a longer timescale, clearly distinct from the reversible inhibition described in detail above. Under conditions in which APEX and APEX2 display fast initial rates of guaiacol oxidation (1 mM H_2O_2 and 1.4 mM guaiacol) the rate of oxidation gradually declines for both enzymes until no activity remains (Supplementary Fig. 16). This pattern is consistent with previous observations of irreversible peroxidase inactivation[9] and is different from the reversible inhibition described above, in which APEX initially displays a slow rate that is maintained for several minutes. We tested whether the inhibition of APEX2 under these conditions could be reversed by addition of excess guaiacol (30 mM) (Supplementary Fig. 16C). No activity was observed, but when fresh enzyme was added to the cuvette, rapid guaiacol oxidation resumed.

We therefore conclude that, while APEX2 is more resistant than APEX to reversible H_2O_2 inhibition, both peroxidases are similarly susceptible to irreversible inactivation. Both enzymes turn over ~3000-4000 times before becoming permanently inactivated in the presence of 1 mM H_2O_2 and 1.4 mM guaiacol. In contrast, HRP gives >130,000 turnovers under these conditions. Thus one molecule of HRP is capable of generating far greater signal than one molecule of APEX2. We have not elucidated the mechanism of irreversible inhibition, but one possibility is the reaction between H_2O_2 and Compound I.[10] Previous studies have suggested that HRP's intrinsic catalase activity (Supplementary Fig. 12)[11] may contribute to its H_2O_2 resistance by accelerating Compound I depletion, thereby minimizing undesired reactions between Compound I and H_2O_2 that lead to irreversible inactivation.[11] In contrast to HRP, wild-type APX, the enzyme from which APEX and APEX2 are derived, has no catalase activity.[12] It would be interesting if engineering such activity into APEX2 could improve its resistance to irreversible H_2O_2 inactivation as well. Another possible mechanism of irreversible inhibition that we cannot rule out is attack by phenoxyl radicals on the heme co-factor and/or the protein itself.[13]

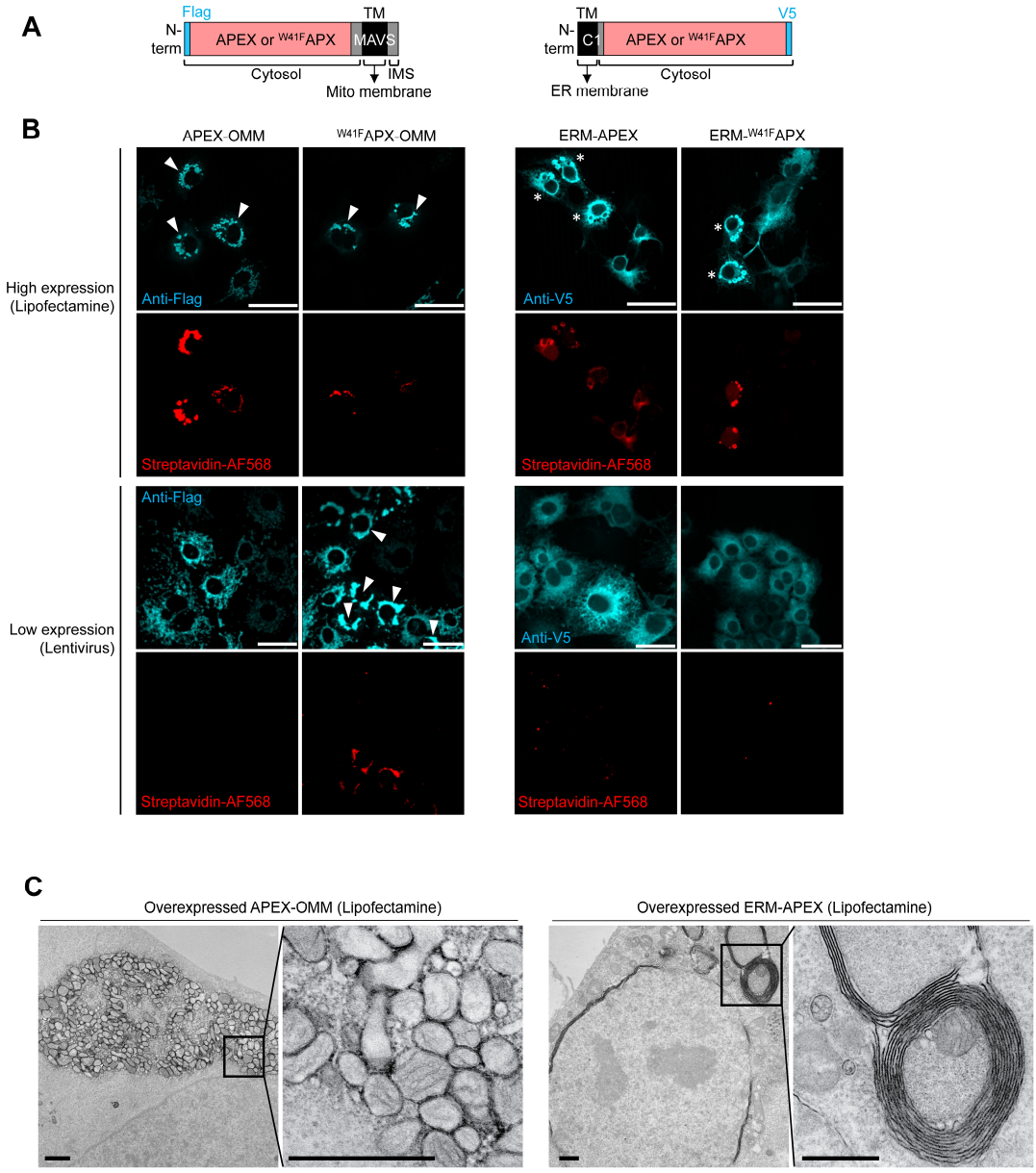

Supplementary Figure 1. APEX activity is undetectable at low expression levels, while high expression causes aggregation of mitochondrial and endoplasmic reticulum (ER) membranes. (**A**) Domain structures of fusion constructs used to target APEX to the outer mitochondrial membrane (OMM) (left) and ER membrane (ERM) (right). In each case, APEX is anchored by a transmembrane (TM) sequence and faces the cytosol. MAVS, C-terminal 31 amino acids of the human mitochondrial antiviral-signaling protein. IMS, intermembrane space. C1, residues 1-27 of the ER-resident P450 oxidase 2C1.[14] (**B**) Fluorescence imaging of OMM- and ERM-targeted APEX at high (top) and low (bottom) expression levels. High expression was achieved via lipofectamine transfection. Low expression was achieved via lentiviral transduction. COS-7 cells expressing the indicated construct were labeled live with biotin-phenol for one minute, then fixed and stained with streptavidin-AlexaFluor568 to visualize biotinylated proteins, and anti-Flag or anti-V5 antibody to visualize APEX expression. The Flag and V5 channel intensities are not normalized between the lipofectamine and lentivirus experiments. For APEX constructs, overexpression gives detectable biotinylation, but causes severe aggregation of mitochondria (arrowheads) and ER (asterisks). When

APEX expression is lowered, biotinylation is no longer detectable. When APEX is replaced by the dimeric ^{W41F}APX, which has higher sensitivity, some biotinylation is seen for the OMM construct at low expression levels, but the dimeric nature of the peroxidase causes mitochondrial aggregation. For the ERM construct, ^{W41F}APX gives normal ER morphology at low expression levels, but biotinylation signal is still absent. Images representative of > 10 fields of view. Scale bars, 50 μm. (**C**) EM images of the mitochondrial and ER aggregates (also previously documented by Snapp *et al*.[15]) observed when OMM- or ERM-targeted APEX is overexpressed as in (B). Dark contrast is caused by APEX activity. Images representative of 5 fields of view. Scale bars, 1 μm.

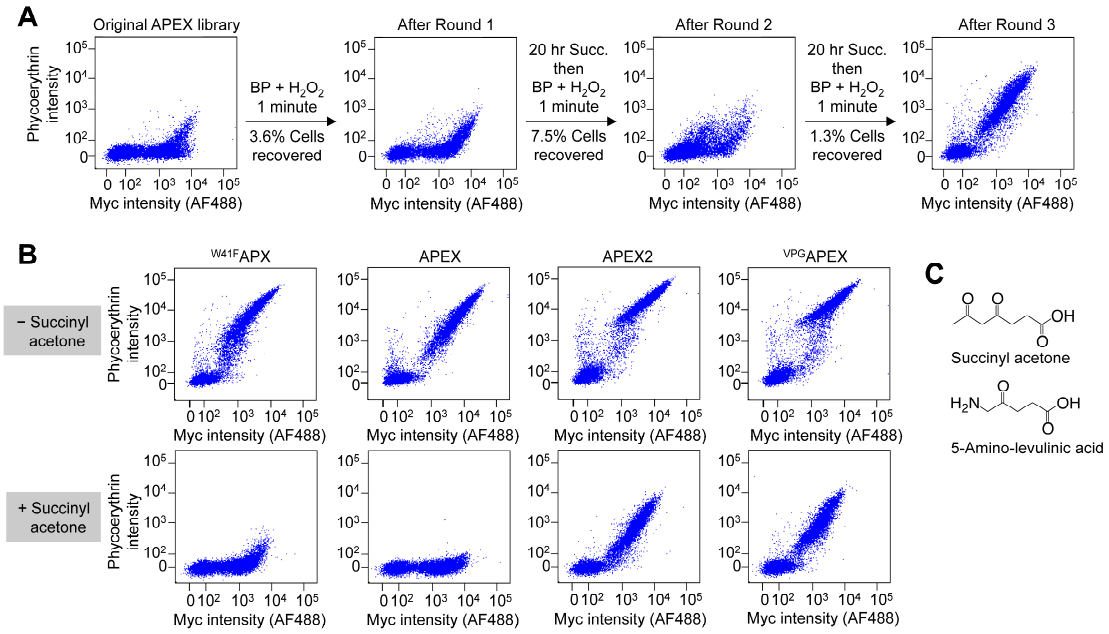

Supplementary Figure 2. FACS analysis of yeast display selections. (**A**) Three rounds of selection were performed, with the labeling conditions used for each round indicated above the arrows. Percentage of input cells recovered in each round indicated beneath the arrows. After each round, selected cells were reamplified and analyzed in parallel under matched conditions. These conditions were 1 minute labeling with biotin-phenol (BP) and H_2O_2, following 20 hr preincubation with succinyl acetone (succ.). Subsequent streptavidin and anti-myc staining were performed as in Figure 1D. Each plot representative of a single trial, n =10,000 cells. (**B**) Analysis of selected yeast clones. Clonal populations of yeast expressing APEX2 or ^{VPG}APEX were labeled and analyzed as in (A). In the bottom row, the same analysis was performed but with 20 hours of succinyl acetone preincubation. For comparison, the starting template APEX and the dimeric peroxidase ^{W41F}APX are also shown. Each plot representative of two trials, n =10,000 cells. (**C**) Structure of the heme biosynthesis inhibitor succinyl acetone, which blocks the processing of 5-aminolevulinic acid, shown below. The use of succinyl acetone in rounds 2 and 3 increased the stringency and hence dynamic range of our selection.

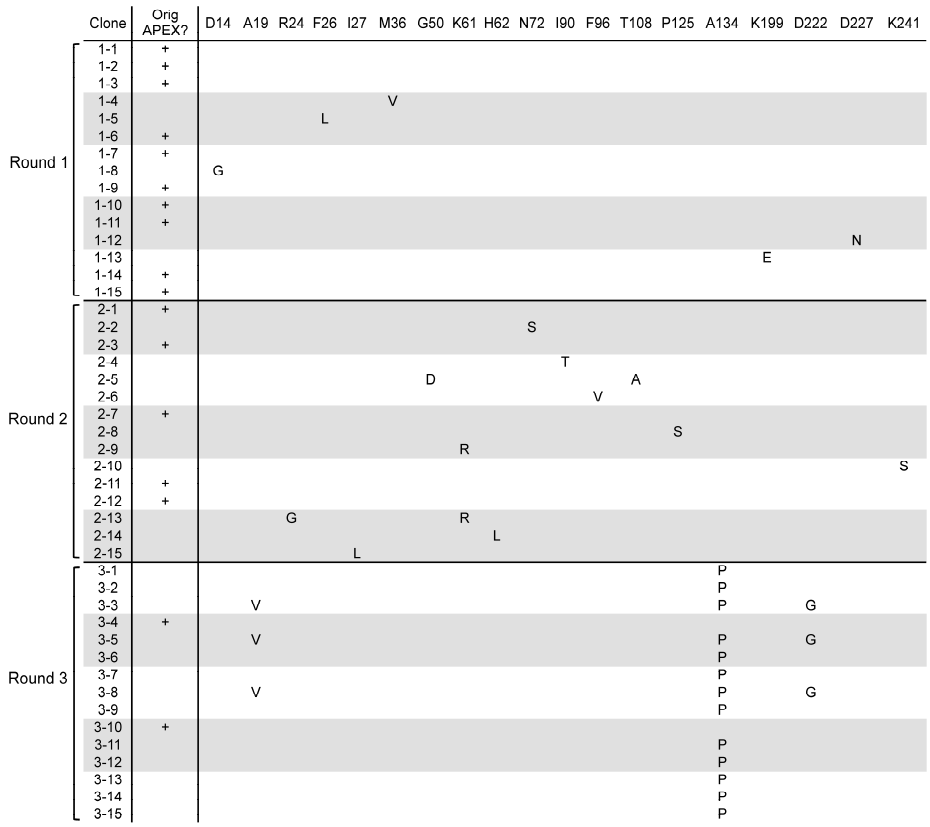

Supplementary Figure 3. Sequencing analysis of yeast display selections. After rounds 1, 2, and 3, DNA from 15 individual yeast colonies were harvested and sequenced. Amino acid mutations observed relative to the APEX starting template are shown. Some clones were identical to the original APEX, as indicated in the second column.

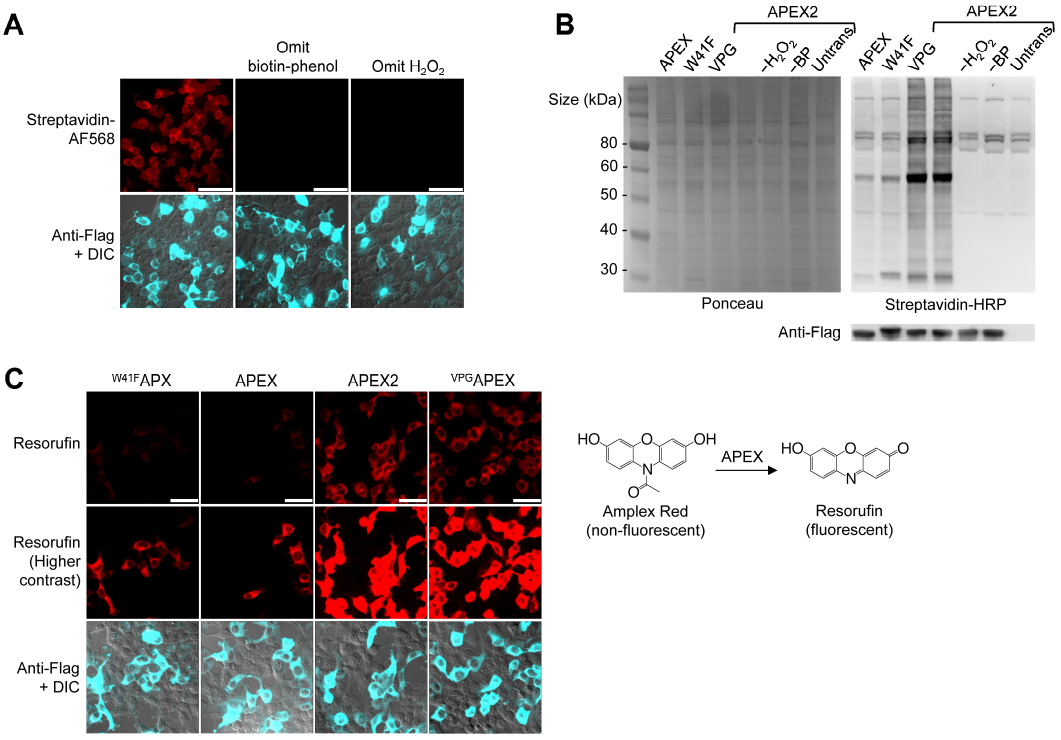

Supplementary Figure 4. Further characterization of APEX2 for proteomic tagging in live cells. (**A**) Negative controls for the cell imaging data shown in Figure 2A. The first column shows biotin-phenol labeling with H_2O_2 as in Figure 2A. The other columns show controls with biotin-phenol or H_2O_2 omitted from the labeling reaction. Images representative of > 10 fields of view. DIC, differential interference contrast. (**B**) Streptavidin blot analysis of whole cell lysate after APEX2 labeling. HEK cells expressing APEX2 in the cytosol were labeled with biotin-phenol as in Figure 2A, then lysed, run on a 9% SDS-PAGE gel, and analyzed by blotting with streptavidin-HRP (right). Negative controls are shown with H_2O_2 omitted, biotin-phenol (BP) omitted, or APEX2 omitted ("untrans"). For comparison, HEK expressing APEX, ^{W41F}APX, or ^{VPG}APEX instead of APEX2 are shown. The Ponceau-stained blot shows equal loading of lysate into gel lanes (left). The anti-Flag blot (below) shows equal expression of APEX variants in HEK cells. Representative of two trials. (**C**) APEX2 is also more active than APEX towards Amplex UltraRed oxidation in live cells. Live HEK expressing APEX2 in the cytosol were incubated with Amplex UltraRed and H_2O_2 for 6 minutes on ice before the cells were fixed and imaged for resorufin fluorescence (the product of Amplex Red oxidation by APEX). Resorufin channels are shown at low and high contrast. Three other APEX variants are shown for comparison. Anti-Flag staining was used to visualize peroxidase expression. Images representative of > 10 fields of view. All scale bars, 50 µm.

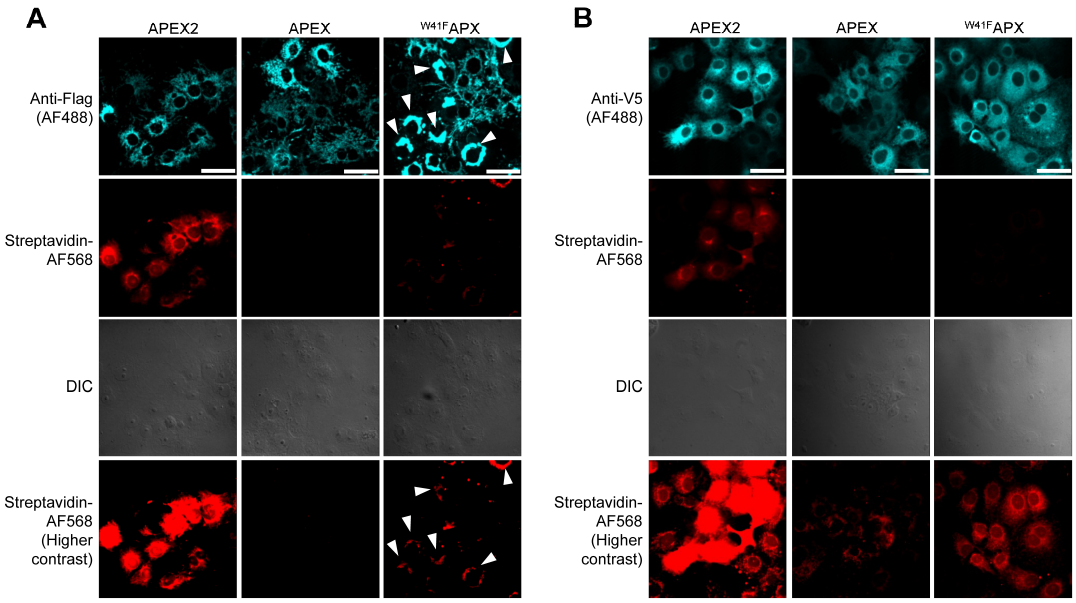

Supplementary Figure 5. High-sensitivity biotinylation of mitochondrial and ER membrane proteomes by APEX2 with minimal organellar perturbation. (**A**) Imaging of mitochondrial outer membrane (OMM) fusion constructs in COS-7 cells. Construct domain structures are shown in Supplementary Figure 1A. Constructs were introduced by lentivirus to maintain low expression levels. Biotin-phenol labeling was performed for 1 minute as in Supplementary Figure 1A. Streptavidin-AlexaFluor568, shown with low and high contrasting, highlights biotin labeling sites. Anti-Flag antibody detects the Flag epitope in APEX-OMM. In the ^{W41F}APX column, mitochondrial aggregates are indicated by arrowheads. (**B**) Same as (A), but with APEX variants targeted to the ER membrane (ERM), facing the cytosol. Construct domain structures are shown in Supplementary Figure 1A. Anti-V5 antibody detects the V5 epitope in ERM-APEX. DIC, differential interference contrast, not normalized. All scale bars, 50 µm. Images representative of > 10 fields of view.

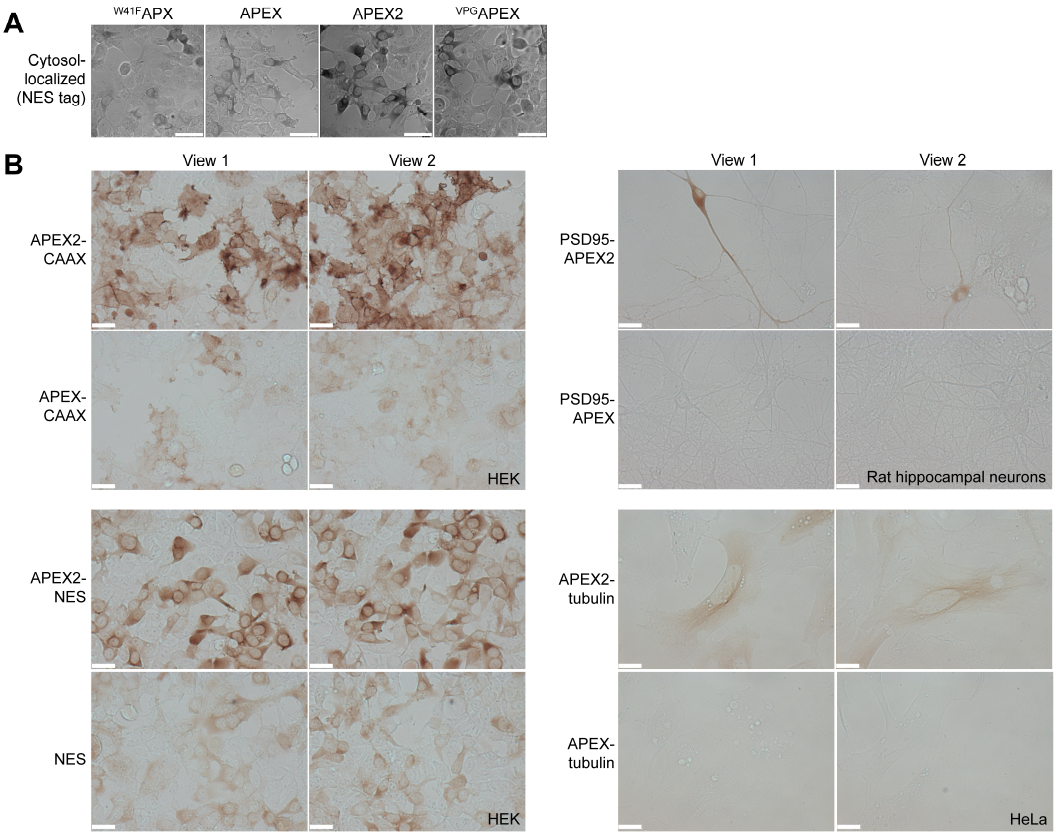

Supplementary Figure 6. APEX2 has improved cellular activity for DAB polymerization for EM. (A) Cytosol-localized APEX variants were expressed in HEK, fixed, and stained with diaminobenzidine (DAB) for 5 minutes. Cells were imaged in brightfield mode, where dark regions indicate areas with dense DAB polymer deposits. Scale bars, 50 µm. (**B**) APEX/APEX2 fusion construct pairs targeting the plasma membrane (CAAX), cytosol (NES), PSD95, and α -tubulin were transfected into the indicated cell type. Cells were fixed and stained with DAB for 5 minutes, except for the tubulin samples which were stained for 10 minutes. Separate immunofluorescence controls showed similar expression levels between APEX and APEX2 construct pairs (data not shown). Scale bars, 270 µm. Each image is representative of >10 fields of view.

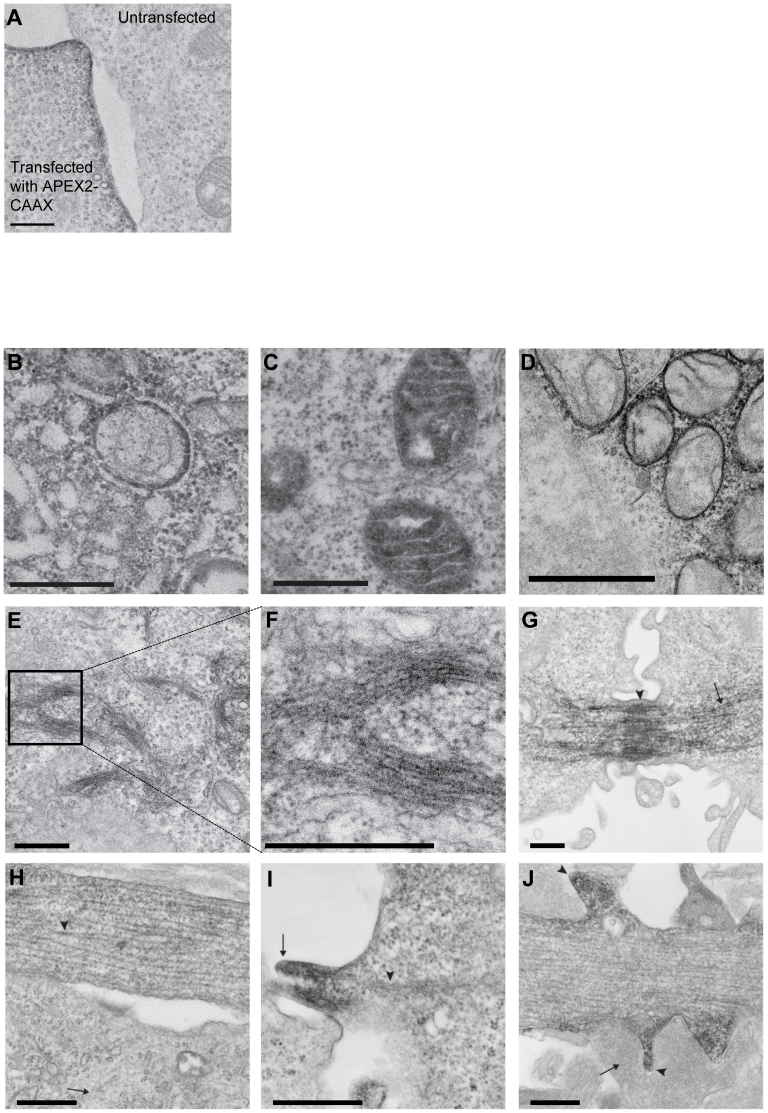

Supplementary Figure 7. Additional EM images with APEX2. (A) Control EM image for Figure 2D showing the plasma membrane contrast in an untransfected HEK293T cell beside a cell expressing APEX2-CAAX. (B)-(J) APEX2 can be used to visualize proteins and organelles in multiple cell types. (**B**) APEX2-syntaxin 17 in HEK (lentiviral transduction) shows dark stain between mitochondria and ER tubules. (**C**) ATP5J-APEX2 in HEK (lipofectamine transfection). (**D**) APEX2-OMM (domain structure in Supplementary Figure 1A) in HEK (lentiviral transduction). (**E**)-(**F**) APEX2-vimentin in HEK (lipofectamine transfection). (**G**) APEX2-α-tubulin in HEK (lipofectamine transfection). In polymerized tubulin, APEX2 faces into the hollow core of microtubules. Dark stain is visible in filaments (arrow) and in the midbody (arrowhead) of a mitotic cell. (**H**) APEX2-α-tubulin in cultured DIV18 rat hippocampal neurons (lentivirus with synapsin promoter). Dark filaments are visible in APEX2-expressing neurons (arrowhead), while microtubules in non-expressing or lower-expressing neurons are light by comparison (arrow). (**I**) APEX2-β-actin in HEK (lipofectamine transfection). Dark stain is observed on actin filaments (arrowhead) and within filopodia (arrow). (**J**) APEX2-β-actin in cultured DIV18 rat hippocampal neurons (lentivirus with synapsin promoter). Dark stain is observed in dendritic spines (arrowheads), consistent with previous studies of β-actin localization in hippocampal neurons.[16] Arrow points to presynaptic vesicles. All scale bars, 500 nm.

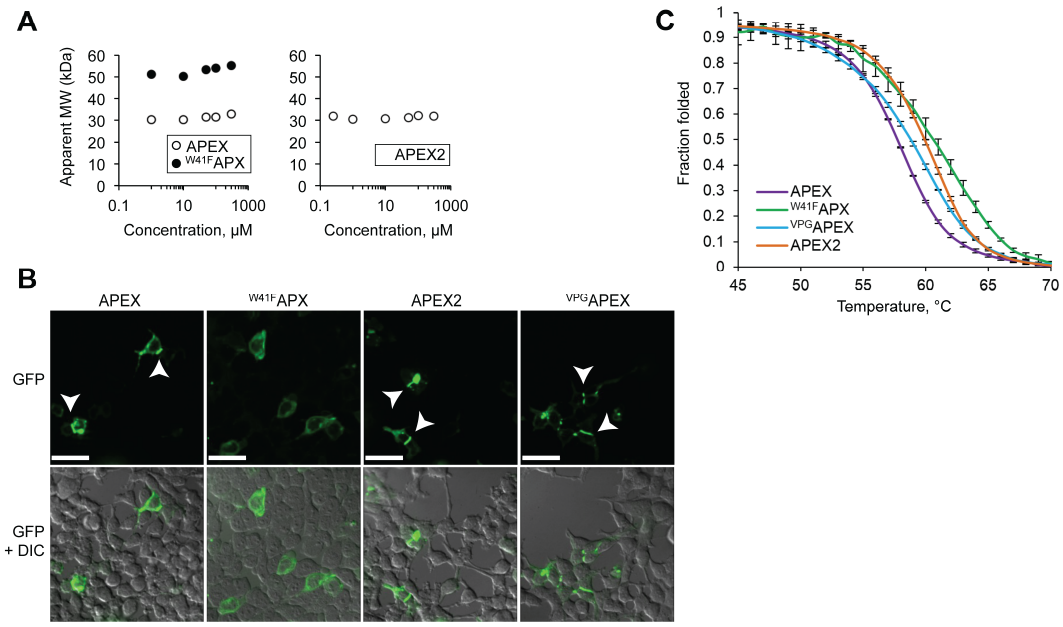

Supplementary Figure 8. Analysis of APEX2 monomericity and thermal stability. (**A**) Gel filtration analysis of APEX2 (right), and APEX and ^{W41F}APX (left). Protein concentrations ranged from 1-300 μM. Protein elution was detected by absorbance at 280 nm. Apparent molecular weights (MW) were calculated as described in Materials and Methods. ^{W41F}APX ran as a dimer at all concentrations tested, whereas APEX and APEX2 ran as monomers (apparent MW ≈ actual MW of 28 kD). Plots are from a single trial. (**B**) Imaging of connexin43 fusion constructs. Connexin43 is sensitive to the oligomerization state of the protein to which it is fused. Dimeric fusion proteins prevent connexin43 from forming gap junctions[17]. GFP followed by APEX2 was fused to the C-terminus of connexin43. Images of GFP fluorescence were recorded in live HEK 293T cells. Arrowheads point to connexin43-containing gap junctions between pairs of transfected cells. Fusions to ^{W41F}APX, APEX, and ^{VPG}APEX are shown for comparison. GFP fluorescence intensity is not normalized across columns. Scale bars, 50 μm. Images representative of > 10 fields of view each. (**C**) Thermal stabilities of APEX variants. Purified proteins, each at 6.1 μM, were heated while heme absorbance at 405 nm was measured. Protein unfolding results in loss of heme which reduces 405 nm absorbance[18]. Fraction folded on the y-axis is defined as $(Abs_{obsvd} - Abs_{min})/(Abs_{max} - Abs_{min})$. Each curve represents the average of three independent measurements. Error bars, ± 1 s.d.

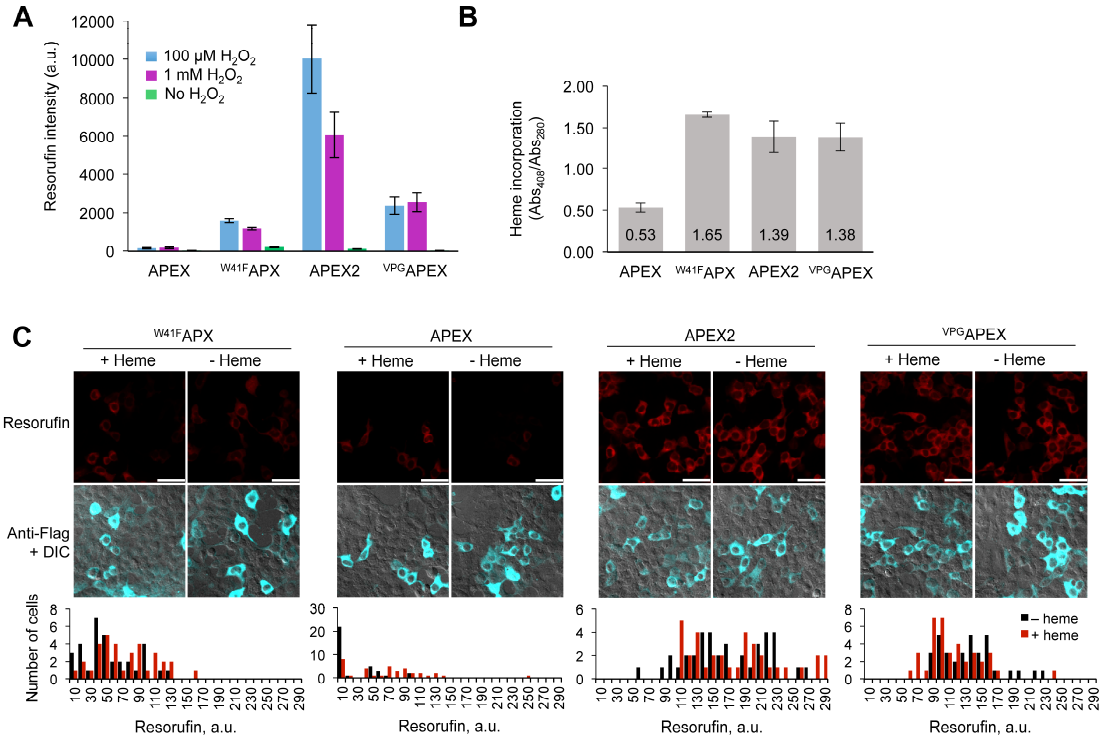

Supplementary Figure 9. Heme occupancy of APEX variants. (**A**) APEX2 is more active than APEX in living *E. coli*. Each APEX variant shown was expressed in *E. coli* BL21 via IPTG induction. Amplex UltraRed and H_2O_2 (1 mM, 100 μM, or 0 μM) were added to 10^8 live cells for 1 minute, then resorufin fluorescence was measured using a fluorescence platereader. Intensities represent the average of three independent replicates. Error bars, ± 1 s.d. Separate experiments showed that peroxidase expression levels were comparable across samples except for dimeric ^{W41F}APX, whose expression was consistently >2x that of APEX2 (data not shown). Normalizing for this, the difference in activity between APEX2 and ^{W41F}APX is even greater than what is shown here (in favor of APEX2). (**B**) Comparison of heme incorporation levels for APEX variants expressed in and purified from *E. coli*. Expression was induced at 37 °C for 22 hours. Peroxidases were then harvested and purified via His_6-tag chromatography. The ratio of absorbance at 408 nm versus 280 nm reflects the heme to protein ratio. Each ratio represents the average of three independent protein preparations. Separate calibrations showed that a ratio of 2.0 corresponds to 57% heme occupancy in APEX (see Methods). (**C**) Indirect analysis of heme occupancy in mammalian cells. HEK 293T cells expressing the indicated APEX variant (targeted to the cytosol via fusion to an NES tag) were labeled with Amplex UltraRed as in Supplementary Figure 4C, with or without prior incubation for 22 hrs with 7 μM heme. Anti-Flag immunostaining was performed after cell fixation to quantify APEX expression levels. Images representative of > 10 fields of view. Scale bars, 50 μm. Histograms below each image set show the distribution of single-cell mean resorufin intensities (>30 cells for each condition). Black and red histograms show the –heme and +heme data, respectively. By the Wilcoxon rank sum test, APEX and ^{W41F}APX, but not APEX2, show significant shifts in intensity values when comparing +/- heme conditions ($p < .00004908$, 0.0379, and 0.7530 for APEX, ^{W41F}APX, and APEX2 respectively), suggesting that the former start with lower heme occupancy, while APEX2 is heme-saturated and does not benefit from further incubation with free heme.

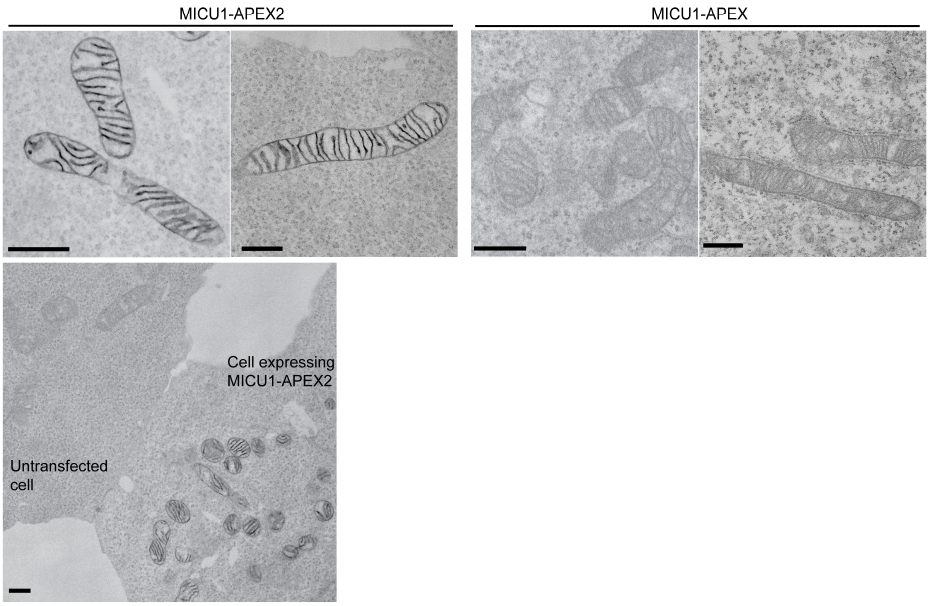

Supplementary Figure 10. EM visualization of MICU1 requires APEX2. In previous experiments, we found that overexpression of MICU1-APEX led to mislocalization of MICU1 on the outside of mitochondria (observed at the EM level, data not shown). Here, we expressed MICU1-APEX2 (left) and MICU1-APEX (right) in parallel via lentiviral transduction, to maintain low expression levels, in HEK. After fixation, DAB staining was performed for 5 minutes. EM shows dark stain in the mitochondrial intermembrane space for MICU1-APEX2, whereas the MICU1-APEX sample is indistinguishable from untransfected cells (bottom). The low sensitivity of APEX, plus the intolerance of MICU1 for overexpression, precludes the use of APEX for EM visualization of MICU1. Scale bars, 500 nm. Images representative of > 6 fields of view each.

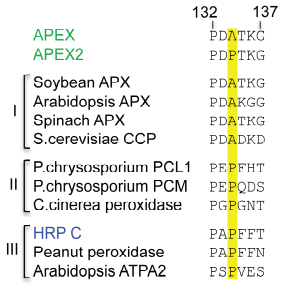

Supplementary Figure 11. Alignment of heme peroxidase sequences. The sequences of all 8,936 Class I, II, and III peroxidases available from Peroxibase (http://peroxibase.toulouse.inra.fr/index.php)[4] were retrieved and aligned with wild-type ascorbate peroxidase using Clustal Omega. Substrate binding loop sequences for wild-type ascorbate peroxidase (soybean APX), APEX, APEX2, horseradish peroxidase (HRP C), and other representative Class I, II, and III peroxidases are shown. Residue numbering relative to soybean APX. Residue 134 is highlighted yellow.

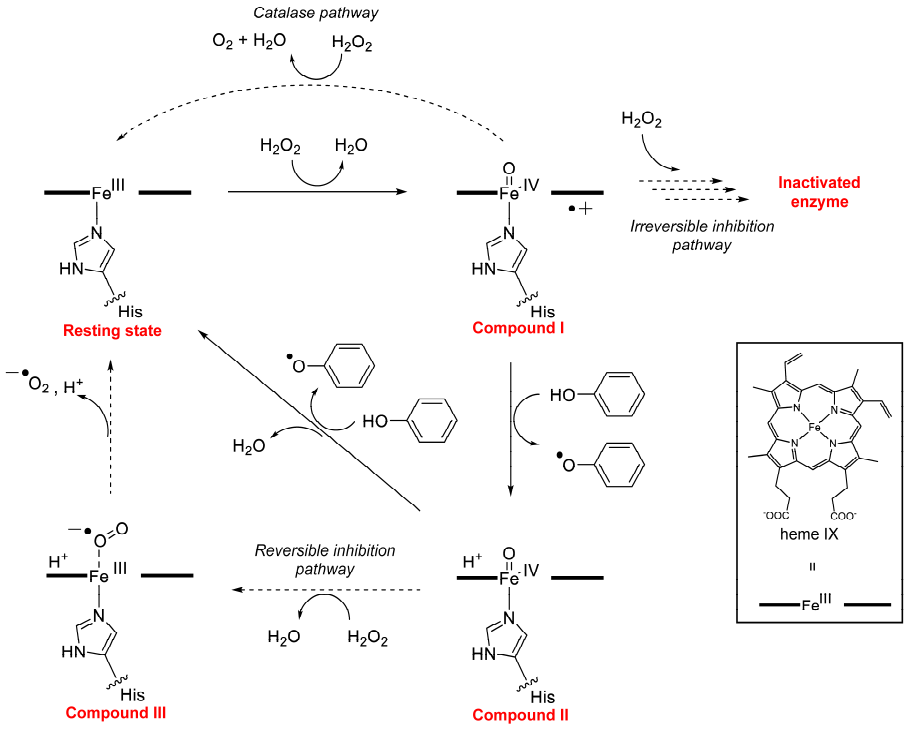

Supplementary Figure 12. Overview of the catalytic and inhibition pathways for heme-containing plant peroxidases. In the productive catalytic pathway, the resting ferric enzyme (Fe^{3+}) reacts with H_2O_2 to form a high-valent iron-oxo intermediate called Compound I, which contains iron (IV) heme with a radical cation on the porphyrin ring. Next, a phenolic substrate binds to the active site of the enzyme, then donates one proton and one electron to Compound I, yielding a phenoxyl radical, which is released from the active site, and Compound II, equivalent to Compound I without the radical cation on the porphyrin ring. Finally, a second equivalent of the phenolic substrate binds to the active site, donating a proton and electron to yield a second phenoxyl radical and returning the enzyme to the ferric resting state. Several side-reactions involving H_2O_2 can occur. These pathways are shown with dotted arrows in the figure and are described in detail in the Supplementary Discussion.

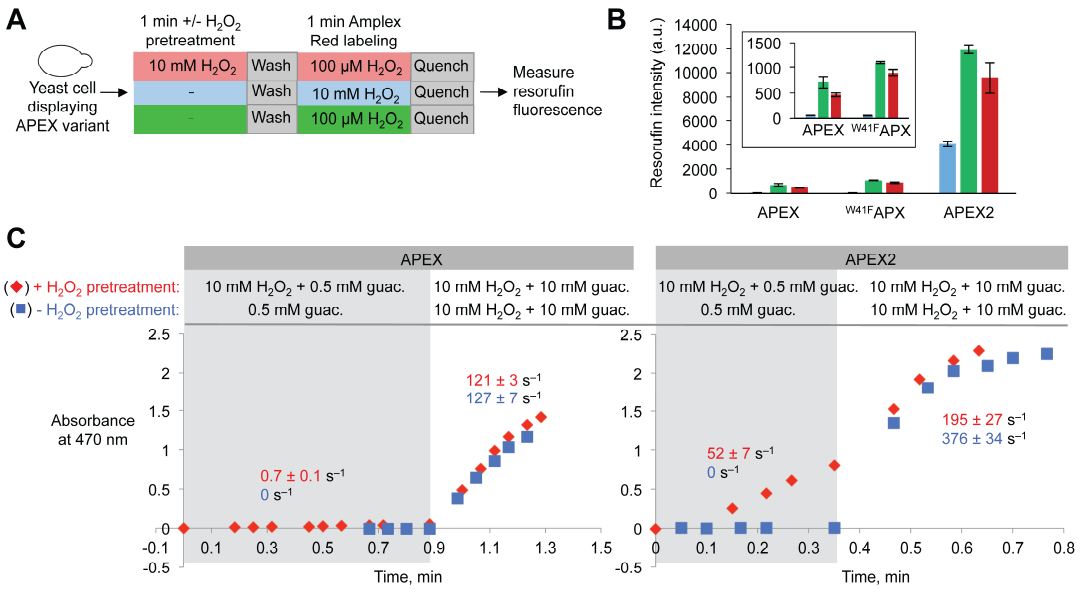

Supplementary Figure 13. APEX2 is more resistant to reversible H_2O_2 inhibition than APEX. (**A**) Scheme for reversibility assay performed on the surface of living yeast cells. APEX, ^{W41F}APX, or APEX2 were expressed on the yeast surface as fusions to Aga2p as in Figure 1D. 10 mM H_2O_2 was added to ~1.25 x 10^5 cells for 1 min, then Amplex UltraRed labeling was performed for 1 minute in the presence of 100 µM H_2O_2 (top row, red). Reference samples (middle and bottom rows) omit the 10 mM H_2O_2 pretreatment. Fluorescence intensity of the supernatant was quantified on a fluorescence platereader. **(B)** Fluorescence intensity data from yeast assay in (A). Data points represent the mean ± 1 s.d. for 3 independent experiments. (**C**) Reversibility assay on purified APEX and APEX2. Peroxidases were initially treated with 10 mM H_2O_2 and 0.5 mM guaiacol (light grey region of graph); APEX turnover was severely inhibited under these conditions, whereas APEX2 turnover was not (red data points). Next, 10 mM guaiacol was added into the same reaction mixture (white region of graph). The rationale was that excess guaiacol may promote the reversion of inhibited APEX/APEX2, as excess veratryl alcohol does for lignin peroxidase[19]. Formation of the tetraguaiacol reaction product was monitored by absorbance at 470 nm. In a control experiment, H_2O_2 was omitted during the pre-treatment phase (blue data points). Values shown on the graphs are initial rates divided by enzyme concentration (40 nM in the pre-treatment phase and 20 nM in the second phase). These represent the mean ± 1 s.d. for 4 independent experiments. Note that for APEX, reaction rate in the second phase is not significantly changed by pre-incubation with high H_2O_2. For APEX2, high H_2O_2 pretreatment causes some drop in reaction rate because *irreversible* H_2O_2-induced inactivation starts to contribute at high turnover numbers.

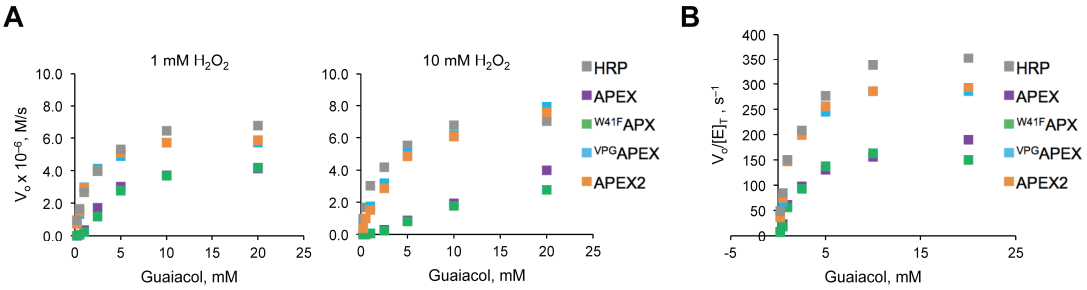

C

Peroxidase	k_{cat} (s^{-1})	K_m (mM)	k_{cat}/K_m ($M^{-1}s^{-1}$)	k_{cat}/K_m rel. to APEX
APEX	230 ± 13	3.8 ± 0.6	6.1 x 10^4	1.00
^{W41F}APX	189 ± 33	3.2 ± 1.0	5.9 x 10^4	0.97
APEX2	299 ± 13	1.7 ± 0.1	1.8 x 10^5	2.95
^{VPG}APEX	310 ± 14	1.9 ± 0.1	1.6 x 10^5	2.62
HRP	358 ± 12	1.5 ± 0.1	2.4 x 10^5	3.93

Supplementary Figure 14. Kinetic characterization of APEX variants. (**A**) Plots showing initial rates (V_o) of peroxidase-catalyzed oxidation of the model phenolic substrate guaiacol. Formation of the oxidation product, tetraguaiacol, was monitored by absorbance at 470 nm. Measurements were performed in the presence of 1 mM (left) or 10 mM (right) H_2O_2. Enzyme concentrations were 20 nM. Though initial rates for HRP, APEX2, and ^{VPG}APEX are similar at both H_2O_2 concentrations, APEX and ^{W41F}APX show significantly diminished rates at higher [H_2O_2] due to H_2O_2-induced inhibition. Data points representative of 2-4 independent measurements. (**B**) Michaelis-Menten curves used to derive the kinetic constants shown in (C). Experiment is the same as in (A) except that each peroxidase was evaluated at its own optimal H_2O_2 concentration: 90 µM for APEX and ^{W41F}APX; 1 mM for APEX2 and ^{VPG}APEX; and 10 mM for HRP. These H_2O_2 concentrations give the highest V_{max} for each peroxidase, while allowing Michaelis-Menten behavior with respect to guaiacol (see Materials and Methods). Enzyme concentration was 20 nM for all data points except when APEX/^{W41F}APX were analyzed at 5, 10, and 20 mM guaiacol (10 nM, 10 nM, and 5 nM enzyme were used, respectively, in order to avoid overly-rapid depletion of H_2O_2). $[E]_T$, total enzyme concentration. Data points representative of 2-4 independent measurements. (**C**) Kinetic constants obtained with guaiacol. K_m is for guaiacol. Errors, ± 1 s.e.m.

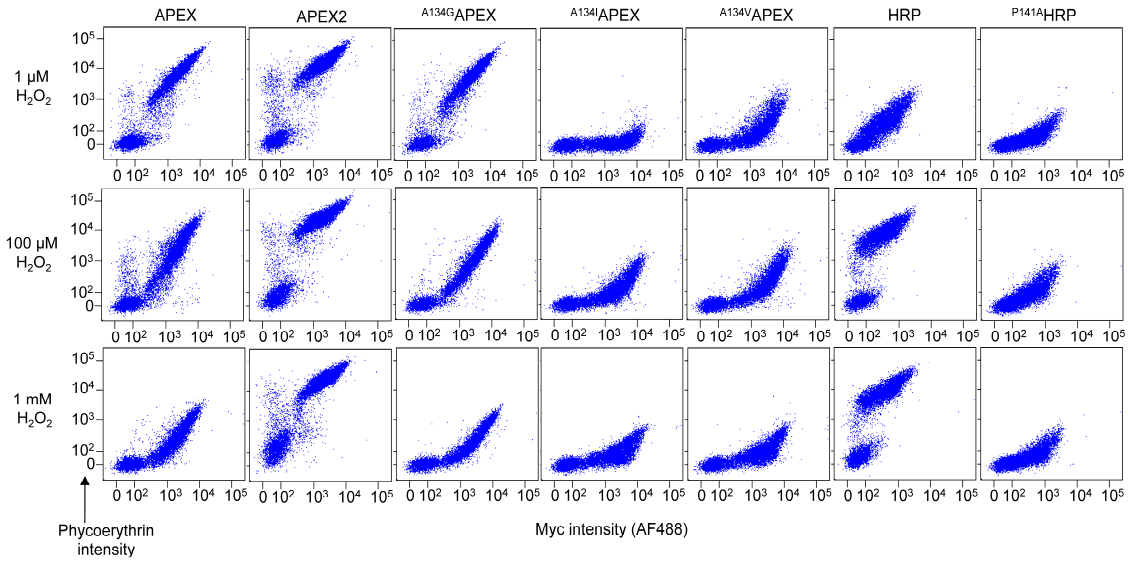

Supplementary Figure 15. Site-directed mutagenesis at residue 134 of APEX and the corresponding position of HRP. The indicated peroxidase mutants were labeled on the yeast surface with 100 μM biotin-phenol and H_2O_2 (1 μM, 100 μM, or 1 mM) for 1 minute, then stained with streptavidin and anti-myc antibody as in Figure 1D. FACS analysis shows activity on the y-axis and expression level on the x-axis. In HRP, residue 141 corresponds to 134 of APEX. Mutation of A134 in APEX to Ile or Val greatly impairs APEX activity, while mutation to Gly has no effect. In HRP, P141A greatly impairs activity, such that the resulting peroxidase is much less active than APEX2 at all H_2O_2 concentrations. Each plot shows 10,000 cells.

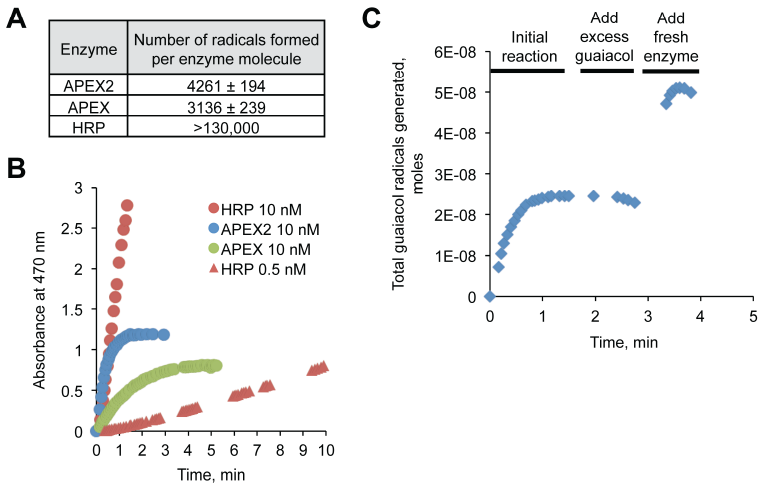

Supplementary Figure 16. APEX and APEX2 are more susceptible to *irreversible* inhibition than HRP. (**A**) Number of guaiacol radicals formed per molecule of enzyme prior to stabilization of A_{470} signal, taken to indicate irreversible inhibition. Reactions were assembled with 1.4 mM guaiacol and 1 mM H_2O_2. For APEX and APEX2, data represent the mean ± 1 s.d. of 5 independent experiments with 10 nM enzyme. For HRP, 3 independent experiments were performed using 0.5 nM enzyme. The reactions were terminated after >130,000 turnovers because the solutions became cloudy and measurements unreliable. (**B**) Representative graphs used to derive the values in (A). APEX and APEX2 display fast initial rates, but become completely inhibited within 2-5 minutes. (**C**) The inhibition of APEX2 shown in (B) cannot be reversed by addition of excess guaiacol. An initial 600 µL reaction with 1.4 mM guaiacol and 1 mM H_2O_2, a concentration yielding observable turnover for both APEX and APEX2 (Figure 2E), was allowed to proceed until product formation ceased, as in (B). Next, 400 µL of 30 mM guaiacol was added to the cuvette (C_f = 12.8 mM guaiacol). In contrast to the results in Supplementary Figure 13, addition of high guaiacol failed to restore activity to APEX2. An equivalent amount of fresh enzyme (C_f fresh enzyme = C_f initial enzyme = 6 nM) was subsequently added to the cuvette to confirm that the cessation of peroxidase turnover is not due to reactant depletion.

Supplementary Methods

Plasmids and cloning

Genes were cloned into the specified vectors using standard enzymatic restriction digest and ligation with T4 DNA ligase. All APX variants were derived from soybean ascorbate peroxidase. The nuclear export sequence, NES, (LQLPPLERLTLD) was derived from residues 6-17 of the HIV-1 Rev protein.[20] Human MICU1 and MAVS (C-terminal 31 residues, RPSPGALWLQVAVTGVLVVTLLVVLYRRRLH)[21] were used, while the ER-targeted C1 sequence was derived from the N-terminal 27 amino acids of rabbit P450

C1 (MDPVVVLGLCLSCLLLLSLWKQSYGGG).[14] Cx43-GFP-APEX2 and APEX2-NES are available on Addgene (49385 and 49386, respectively).

Plasmid vector	APX variants	For expression in	Epitope tag	Notes
pCTCON2-APX	APEX, ^{W41F}APX, APEX2, ^{VPG}APEX	Yeast	HA: N-term c-Myc: C-term	
pcDNA3-APX-NES	APEX, ^{W41F}APX, APEX2, ^{VPG}APEX	Mammalian	FLAG: N-term	
pLX304-C1(1-27)-APX	APEX, ^{W41F}APX, APEX2	Mammalian	V5: C-term	Lentiviral vector
pLX304-APX-MAVS	APEX, ^{W41F}APX, APEX2	Mammalian	FLAG: N-term	Lentiviral vector
pLX304-MICU1-FLAG-APX	APEX, APEX2	Mammalian	FLAG: linker	Lentiviral vector
pEGFP-APX-Tubulin	APEX, APEX2	Mammalian	FLAG: N-term	
pcDNA3-Cx43-GFP-APX	APEX, ^{W41F}APX, APEX2, ^{VPG}APEX	Mammalian	--	
FCW-APX-Stx17	APEX2	Mammalian	V5: C-term	Lentiviral vector. Derived from FCGW.
FSW-PSD95-V5-APX	APEX, APEX2	Neuronal	V5: linker	Lentiviral vector. Derived from FCGW with human synapsin1 promoter replacing CMV
pcDNA3-APX-CAAX	APEX, APEX2	Mammalian	FLAG: N-term	
pcDNA3-ATP5J-APX	APEX2	Mammalian	V5: C-term	
pTRC99A-APX	APEX, ^{W41F}APX, APEX2, ^{VPG}APEX	Bacterial	His_6: N-term	

Yeast cell culture

S. cerevisiae strain EBY100 was cultured according to previously published protocols.[22] Cells were propagated at 30°C in yeast extract peptone dextrose (YPD) complete media. Transformed cells containing the Trp1 gene were selected on synthetic dextrose plus casein amino acid (SDCAA) plates and propagated in SDCAA media at 30°C. Protein expression was induced by inoculating 4.5 mL of

SGCAA (SDCAA media with dextrose replaced by an equivalent amount of galactose) with 500 µL of a saturated SDCAA yeast culture, and incubating at 30°C for 20-24 hours. Yeast cells were transformed with the yeast display plasmid pCTCON2[22] using the Frozen E-Z Yeast Transformation II Kit (Zymoprep) according to manufacturer protocols.

Generation of APEX library for yeast display

A library of APEX mutants was generated by error-prone PCR according to published protocols [23]. In brief, 150 ng of the template soybean APEX in vector pCTCON2 [22] was amplified for 10 rounds with 0.4 µM forward and reverse primers, 2 mM $MgCl_2$, 5 units of *Taq* polymerase (NEB), and 2µM each of the mutagenic nucleotide analogues 8-oxo-2'-deoxyguanosine-5'triphosphate (8-oxo-dGTP) and 2'-deoxy-p-nucleoside-5'-triphosphate (dPTP). The PCR product was then gel-purified and re-amplified for another 30 cycles under normal PCR conditions. The inserts were then electroporated into electrocompetent *S. cerevisiae* EBY100 [23] with the BamHI-NheI linearized pCTCON2 vector (10 µg insert: 1 µg vector) backbone. Transformation efficiency was 1.2×10^6. DNA sequencing of 16 distinct colonies showed an average of 1 amino acid mutation per clone with a range from 0-4. The electroporated cultures were rescued in 100 mL of SDCAA media supplemented with 50 units/mL penicillin, and 50 µg/mL streptomycin for two days at 30°C.

Yeast display selections

Yeast cultures in SGCAA media [22] were pelleted at 500g for 4 minutes at 4°C and resuspended in an equivalent volume of Dulbecco's Phosphate Buffered Saline (137.9 mM NaCl, 2.7 mM KCl, 8.1 mM Na_2HPO_4, 1.5 mM KH_2PO_4, 0.9 mM $CaCl_2$, 0.5 mM $MgCl_2$, pH 7.4) + 0.1% BSA (1 mg/mL) (DBPS-B). All subsequent work was done using DPBS-B with cultures at 4°C. Cultures were washed once more and the OD_{600} for a 1/100 dilution of the culture was measured. 2.5×10^6 yeast cells (1 $OD_{600} \sim 1 \times 10^7$ yeast cells) were pelleted in a 1.5 mL microcentrifuge tube at 14,000g for 30 seconds. Yeast cells were then resuspended with 1 mL of labeling solution consisting of 100 µM biotin-phenol and 1 µM H_2O_2 and transferred to a 15 mL conical. After 1 minute total reaction time, the solution was quenched with 1 mL of 10 mM Trolox and 20 mM sodium ascorbate followed by rapid vortexing. The cells were pelleted at 14,000g for 1 minute. Excess solution was removed and samples were transferred back to 1.5 mL microcentrifuge tubes. Each sample was washed twice with 125 µL DPBS-B and pelleted. Samples were then resuspended in 50 µL of a 1:50 dilution of mouse α-c-Myc (Calbiochem) and incubated at 4°C with rotation for 1 hour. Samples were washed twice with 125 µL DPBS-B, and resuspended in 50 uL of a 1:50 dilution of streptavidin-phycoerythrin (Jackson ImmunoResearch) and a 1:100 dilution of Alexa Fluor 488 goat anti-mouse IgG (Life Technologies). After 1 hour incubation with rotation at 4°C, samples were washed twice and resuspended in 500 µL PBS-B for FACS analysis.

At least a ten-fold excess of cells relative to the original library diversity were labeled in 2.5×10^6 cell aliquots each round to ensure oversampling. To prepare the cultures, 500 µL of cells grown for 24-48 hours in SDCAA media at 30°C was added to 4.5 mL SGCAA media with or without 1 mM succinyl acetone (succ) for 20 hours at 30°C before labeling as described above.

For FACS sorting, 500 µL samples in DPBS-B were sorted on a BD FACS Aria IIu cell sorter with the 488 nm laser and appropriate emission filters (530/30 for AF488, 575/26 for PE). Gates were drawn to collect yeast cells positive for AF488 signal that also had high PE signal. After sorting, yeast cells were collected in 500 µL – 1mL SDCAA media containing 1% penicillin-streptomycin and incubated at 30°C for 24 hours. 250 µL of the growing culture was removed for DNA extraction, with the rest transferred to 5 mL of SDCAA media + 1% pen-strep for another 24 hours at 30°C. 500 µL of the saturated SDCAA yeast culture was then transferred to SGCAA media to induce protein expression for 20 hours at 30°C before labeling for the next round of selection.

FACS analysis of yeast

Yeast samples were taken from picked colonies of transformed clones, or from each library generation, re-cultured in SDCAA and SGCAA media, and analyzed on a BD LSR II flow cytometer (BD Biosciences). Labeling was performed as described above.

Mammalian cell culture

Hippocampal neurons were harvested from rat embryos sacrificed at embryonic day 18 and plated in 24-well plates as previously described.[24] Neurons were transfected at DIV 9 with 1 µL Lipofectamine 2000 and 200 ng DNA per well for 3 hours in 250 µL MEM. After four days, cells were either fixed and immunostained or fixed and stained with DAB as described above.

Lentiviral infection with APEX fusions

HEK 293T cells in 6-well plates were transfected at ~60-70% confluency with the lentiviral vector pLX304 containing the gene of interest (1000 ng), the lentiviral packaging plasmids dR8.91 (900 ng) and pVSV-G (100 ng) [25], and 10 µL of Lipofectamine 2000 for 3 hours. About 60 hours after transfection, the cell media containing lentivirus was harvested, filtered through a 0.45 µm filter, and added to other fresh cell cultures to induce expression of the gene of interest. Typically for both COS-7 and HEK 293T cultures in wells of a 48-well plate (.95cm^2 per well), cells would be pre-plated the night before at ~50% confluency. The next day, the media would be exchanged for 187.5 µL of fresh media and 62.5 µL of viral media. Cells were then incubated for 48 hours at 37°C with 5% CO_2 before labeling and imaging. For infection of hippocampal neurons, cell culture was performed as described above, and 300 uL of viral media were added at DIV14 to the existing culture media (~2.5 mL). Neurons were fixed and labeled at DIV18.

Sequencing analysis of yeast clones

Plasmid DNA from yeast cultures was harvested from yeast growing at low log-phase using the Zymoprep Yeast Plasmid Miniprep II Kit (Zymo Research) according to the manufacturer's instructions. 4 µL of the purified DNA was transformed into XL1Blue *E. coli* cells by heat-shock transformation and rescued for 1 hour at 37°C. The entire culture was then plated on an LB-ampicillin plate and 16-20 colonies were picked for sequencing of individual clones.

Imaging analysis of Amplex Red labeling in mammalian cells with heme supplementation

HEK 293T on glass cover slips were transfected for 3 hrs with Lipofectamine 2000, before media change into complete media +/- 7 µM heme (from a freshly generated stock solution of 483 µM hemin-Cl (Sigma) in 10 mM NaOH) for 22 hours [26]. Afterwards, cells were moved to ice, washed three times with Dulbecco's phosphate-buffered saline (DPBS), then treated with a solution of 50 µM Amplex UltraRed (Molecular Probes) with 0.02% (6.7 mM) H_2O_2 in DPBS according to previously published protocols [27]. Cells were labeled for 6 minutes before washing and fixation. Samples were blocked using 1% (v/v) bovine serum albumin (BSA, Fisher Scientific) in PBS at 4 °C for 30 min, then treated overnight at 4 °C with a 1:500 dilution of mouse-anti-Flag antibody (Agilent) in DPBS with 1% BSA. Cells were rinsed three times in 0.2% Tween in DPBS, then treated with a 1:750 dilution of Alexa Fluor 488 goat anti-mouse IgG (Life Technologies) for 1 hour at 4 °C. Cells were rinsed three times in DBPS-0.2% Tween, then imaged by confocal microscopy.

The background-corrected mean resorufin fluorescence intensity of individual cells with positive α-FLAG staining were obtained for n > 33 cells per condition. Excel was used to plot the mean intensities of each APX variant +/- heme into histograms in Supplementary Figure 9C. The nonparametric Wilcoxon rank sum test was performed for each variant +/- heme using Matlab to determine whether the activity of the two populations of cells +/- heme could be differentiated.

Gel filtration chromatography

Gel filtration was run according to previously published protocols [27]. Purified APX proteins were diluted to the desired concentrations using chilled (4 °C) PBS (137 mM NaCl, 2.7 mM KCl, 10 mM

Na_2HPO_4, 2.0 mM KH_2PO_4, pH 7.4). Enzyme concentrations were calculated based on total protein content (not heme-bound protein). Samples (45 µL) were run on a GE ÄKTA™ FPLC over a Superdex 75 10/300 column (GE Healthcare) that had been pre-equilibrated in PBS, pH 7.4. Samples were run isocratically at 4°C in PBS at a flow rate of 0.5 mL/min. Elution of APX was monitored by absorbance at 280 nm. UNICORN system control software (GE Healthcare) was used for analysis of elution profiles. Apparent MWs were determined by referencing low molecular weight standards (GE).

Temperature-dependent heme dissociation assay

Temperature-dependent heme dissociation experiments were performed using a Cary 3 UV-Vis spectrophotometer (Varian) equipped with a multicell thermal block according to a published procedure [18] with a few modifications. Temperature was increased at a rate of 6 °C/min, and absorbance was measured at 405 nm to monitor heme dissociation from the enzyme active site (free heme has a lower ε_{405} than APEX-bound heme). Data points were collected every 1 °C. Proteins were diluted in PBS pH 7.4 at room temperature to a concentration of 6.1 µM. Enzyme concentrations were calculated based on holo protein content (A_{405}). The visible spectra were normalized and converted to fraction folded using the formula $(A_{obs}- A_{min})/(A_{max}- A_{min})$.

APEX expression and purification from *E. coli*

N-terminal His_6-tagged APX mutants in pTRC expression vectors were overexpressed in *E. coli* cells of strain BL21-DE3. Individual colonies were amplified in 500 mL Luria Broth (LB) supplemented with 10 µg/mL ampicillin and grown to an OD_{600} of 0.5 at 37 °C. Protein expression was induced with 420 µM isopropyl β–D-1-thiogalactopyranoside (IPTG) and supplemented with 1 mM 5-aminolevulinic acid hydrochloride (Sigma) overnight at room temperature to promote higher heme incorporation [28,29]. Protein samples were purified and concentrated according to previously published protocols [27]. Protein samples were flash frozen in liquid N_2 and stored in aliquots at −80 °C. Purity was checked using SDS-PAGE. All purified APX variants had ratios of A_{405}/A_{280} >2.0, which in previous reports was assumed to indicate full heme occupancy [30]. Our experiments indicated that A_{405}/A_{280} = 2.0 corresponds to heme occupancy of approximately 60%, but we nevertheless deemed these samples suitable for *in vitro* kinetic experiments, despite the presence of some apo protein. Concentrations of heme-bound protein were determined based on Soret band absorbance. The Soret band molar extinction coefficients were determined using the heme pyridine chromogen assay [31] to be ε_{405} = 122 mM^{-1} cm^{-1} for APEX and ε_{405} = 128 mM^{-1} cm^{-1} for ^{VPG}APEX. The ε_{405} values obtained for ^{W41F}APX and APEX2 showed high variation and were much larger (up to 180 mM^{-1} cm^{-1}) than published Soret extinction coefficients for ascorbate peroxidase and its mutants. We attributed these abnormally high extinction coefficients to incomplete extraction of heme from the active site upon addition of pyridine. Since ^{W41F}APX is identical to APEX in terms of heme binding residues, and APEX2 is identical to ^{VPG}APEX, we assumed ε_{405} = 122 mM^{-1} cm^{-1} for ^{W41F}APX and ε_{405} = 128 mM^{-1} cm^{-1} for APEX2. Concentrations of total protein content were determined using the Bicinchoninic Acid (BCA) Protein Assay Kit (Pierce).

Guaiacol steady-state kinetic assays

Guaiacol assays were performed on a Nanodrop 2000c UV-vis spectrophotometer (Thermo Scientific) using its cuvette reader. Equal concentrations of purified, heme-bound holoenzyme were used for each experiment. Concentrations of APEX variants were calculated based on holo protein content, as determined using absorbance at 405 nm (see "APEX expression and purification from *E. coli*" section for details). HRP (Sigma) was dissolved into PBS, pH 7.4, from a lyophilized form, and enzyme concentration was calculated using ε_{405} = 100 mM^{-1} cm^{-1}. Guaiacol (Sigma) was diluted in room temperature PBS, pH 7.4, to concentrations ranging from 0.25 to 30 mM. Solutions were agitated at 37 °C for at least 5 minutes, then vortexed thoroughly to ensure the guaiacol was dissolved. H_2O_2 (Sigma) was diluted from stock solutions to the final concentrations indicated in each figure. Concentrations of H_2O_2 stock solutions were determined using ε_{240} = 43.6 M^{-1} cm^{-1} using a Nanodrop 2000c [32]. Reactions were assembled in disposable plastic cuvettes by adding 600 µL guaiacol solution and 1 µL of a stock H_2O_2

solution. Reactions were initiated by addition of enzyme (1-2 µL from a stock solution), followed by manual mixing and immediate monitoring of absorbance at 470 nm. Oxidation to tetraoguaiacol was measured using ε_{470} = 22 mM^{-1} cm^{-1} [33].

For determination of Michaelis-Menten parameters (Supplementary Fig. 14), H_2O_2 concentrations were as follows: 90 µM for APEX and ^{W41F}APX, 1 mM for APEX2 and ^{VPG}APEX, and 10 mM for HRP. A H_2O_2 concentration was selected for each enzyme to give the highest V_{max} while still allowing the enzyme to exhibit Michaelis-Menten behavior with respect to guaiacol. For example, HRP displayed higher v_o using 10 mM H_2O_2 as compared to 1 mM H_2O_2 for all guaiacol concentrations tested, so 10 mM H_2O_2 was used for HRP. On the other hand, although APEX displayed high V_{max} values with 1 and 10 mM H_2O_2, v_o values for guaiacol concentrations < 2.5 mM were highest using 90 µM H_2O_2. The higher k_{cat} values derived here for APEX and ^{W41F}APX as compared to previous work [27] can be accounted for by 3 factors. First, protein concentration in this work was determined based on holo enzyme, whereas the previous work used total enzyme. Second, heme reconstitution was performed in the previous work, but not here. Although heme reconstitution boosts heme occupancy, we have also observed that it decreases specific activity. Third, the previous values were obtained using APEX derived from pea, whereas these values were obtained for soybean-derived enzymes. k_{cat} and K_M were calculated by nonlinear regression fitting of the data in Figure S14B to the Michaelis-Menten equation using OriginPro. Standard errors are calculated in this software based on the Variance-Covariance Matrix and mean residual variance.

For the H_2O_2 titration shown in Figure 2E, the 1.4 mM guaiacol data points for APEX2 and ^{VPG}APEX between 250 µM and 5 mM H_2O_2 represent lower bounds and have large errors because the uninhibited initial rates could not be captured in our assay. Both enzymes exhibited $v_o / [E]_t > 100$ under these conditions, but the rate of product formation had already declined within a few seconds—faster than the time-scale of the manual mixing used in our assay—due to accumulation of inactivated enzyme.

In vivo measurement of heme incorporation in *E. coli* cells

Three individual colonies from plated *E. coli* BL21-DE3 cells expressing each APX variant (APEX, ^{W41F}APX, APEX2, and ^{VPG}APEX) were picked into separate liquid cultures. Each culture was amplified in 100 mL LB supplemented with 10 µg/mL ampicillin at 37°C, and protein expression was induced at an OD_{600} of 0.5 with 420 µM IPTG. Cultures were grown at 37°C overnight for approximately 25 hours. 1 x 10^8 cells per culture were isolated as measured by OD_{600} (0.1 OD_{600} = 2 x 10^7 cells/mL) for characterizing comparative intracellular APX variant activity. Cells were pelleted and resuspended in 200 µL of 50 µM Amplex UltraRed in DPBS, pH 7.4, and specified concentrations of H_2O_2 for 1 minute. The reaction was quickly quenched with addition of 200 µL of a quenching solution (10 mM Trolox, 20 mM sodium ascorbate, 20 mM NaN_3 in DPBS). Cells were pelleted at 14,000g for 1 minute and 150 µL of each supernatant was transferred to a FLUOTRAC 200 96-well plate (Greiner Bio One). Samples were measured for resorufin fluorescence on a Tecan SAFIRE microplate reader, with excitation at 571 nm and emission measured at 585 nm. The rest of the cultures were pelleted and purified as described above. Samples were not concentrated. Heme incorporation was measured as a ratio of A_{408}/A_{280} on a Nanodrop 2000c UV-vis spectrophotometer (Thermo Scientific). As stated in Supplementary Figure 9, we found that a ratio of 2.0 corresponds to 57% heme occupancy in APEX. This number was calculated by determining heme-bound protein concentration in a purified protein sample based on A_{405}, then dividing this number by the total protein concentration, as determined using the BCA assay.

EM imaging

EM imaging of the samples shown in Figure 2D and Supplementary Figures 1C, 7 was performed as previously described.[27] The DAB-stained areas of the embedded cell samples were identified by transmitted light, selectively sawed out using a jeweler's saw and mounted on dummy acrylic blocks with cyanoacrylic adhesive (Krazy Glue, Elmer's Products). The coverslip was removed, the block trimmed, and ultrathin (80 nm thick) sections were cut using an ultramicrotome (Leica Ultracut UTC6). Electron micrographs were recorded using a JEOL 1200 TEM operating at 80 keV.

References

1. A, H. *et al.* Kinetic study of the inactivation of ascorbate peroxidase by hydrogen peroxide. (2000).

2. Arnao, M. B., Acosta, M., del Rio, J. A., Varón, R. & García-Cánovas, F. A kinetic study on the suicide inactivation of peroxidase by hydrogen peroxide. *Biochim. Biophys. Acta - Protein Struct. Mol. Enzymol.* **1041,** 43–47 (1990).

3. Nakajima, R. & Yamazaki, I. The mechanism of oxyperoxidase formation from ferryl peroxidase and hydrogen peroxide. *J. Biol. Chem.* **262,** 2576–2581 (1987).

4. Fawal, N. *et al.* PeroxiBase: a database for large-scale evolutionary analysis of peroxidases. *Nucleic Acids Res.* **41,** D441–4 (2013).

5. Oesterhelt, C., Vogelbein, S., Shrestha, R. P., Stanke, M. & Weber, A. P. M. The genome of the thermoacidophilic red microalga Galdieria sulphuraria encodes a small family of secreted class III peroxidases that might be involved in cell wall modification. *Planta* **227,** 353–62 (2008).

6. Hill, A. P. *et al.* Chemical, Spectroscopic and Structural Investigation of the Substrate-Binding Site in Ascorbate Peroxidase. *Eur. J. Biochem.* **248,** 347–354 (1997).

7. Cosio, C. & Dunand, C. Specific functions of individual class III peroxidase genes. *J. Exp. Bot.* **60,** 391–408 (2009).

8. Hiner, A. N. P. *et al.* Reactions of the class II peroxidases, lignin peroxidase and Arthromyces ramosus peroxidase, with hydrogen peroxide. Catalase-like activity, compound III formation, and enzyme inactivation. *J. Biol. Chem.* **277,** 26879–85 (2002).

9. Arnao, M. B., Acosta, M., del Río, J. A. & García-Cánovas, F. Inactivation of peroxidase by hydrogen peroxide and its protection by a reductant agent. *Biochim. Biophys. Acta* **1038,** 85–9 (1990).

10. Miyake, C. & Asada, K. Inactivation Mechanism of Ascorbate Peroxidase at Low Concentrations of Ascorbate; Hydrogen Peroxide Decomposes Compound I of Ascorbate Peroxidase. *Plant Cell Physiol.* **37,** 423–430 (1996).

11. Hernández-Ruiz, J., Arnao, M. B., Hiner, A. N., García-Cánovas, F. & Acosta, M. Catalase-like activity of horseradish peroxidase: relationship to enzyme inactivation by H2O2. *Biochem. J.* **354,** 107–14 (2001).

12. Hiner, A. N. *et al.* Kinetic study of the inactivation of ascorbate peroxidase by hydrogen peroxide. *Biochem. J.* **348 Pt 2,** 321–8 (2000).

13. Huang, Q. *et al.* Inactivation of horseradish peroxidase by phenoxyl radical attack. *J. Am. Chem. Soc.* **127,** 1431–7 (2005).

14. Szczesna-Skorupa, E. Mobility of cytochrome P450 in the endoplasmic reticulum membrane. *Proc. Natl. Acad. Sci.* **95,** 14793–14798 (1998).

15. Snapp, E. L. *et al.* Formation of stacked ER cisternae by low affinity protein interactions. *J. Cell Biol.* **163,** 257–69 (2003).

16. Kaech, S., Fischer, M., Doll, T. & Matus, A. Isoform Specificity in the Relationship of Actin to Dendritic Spines. *J. Neurosci.* **17,** 9565–9572 (1997).

17. Lauf, U., Lopez, P. & Falk, M. M. Expression of fluorescently tagged connexins: a novel approach to rescue function of oligomeric DsRed-tagged proteins. *FEBS Lett.* **498,** 11–5 (2001).

18. Mandelman, D., Schwarz, F. P., Li, H. & Poulos, T. L. The role of quaternary interactions on the stability and activity of ascorbate peroxidase. *Protein Sci.* **7,** 2089–98 (1998).

19. Wariishi, H. & Gold, M. Lignin peroxidase compound III. Mechanism of formation and decomposition. *J. Biol. Chem.* **265,** 2070–2077 (1990).

20. Wen, W., Meinkoth, J. L., Tsien, R. Y. & Taylor, S. S. Identification of a signal for rapid export of proteins from the nucleus. *Cell* **82,** 463–73 (1995).

21. Seth, R. B., Sun, L., Ea, C.-K. & Chen, Z. J. Identification and Characterization of MAVS, a Mitochondrial Antiviral Signaling Protein that Activates NF-κB and IRF3. *Cell* **122,** 669–682 (2005).

22. Chao, G. *et al.* Isolating and engineering human antibodies using yeast surface display. *Nat. Protoc.* **1,** 755–68 (2006).

23. Colby, D. W. *et al.* Engineering Antibody Affinity by Yeast Surface Display. *Methods Enzymol.* **388,** 348–358 (2004).

24. Liu, D. S., Loh, K. H., Lam, S. S., White, K. A. & Ting, A. Y. Imaging trans-cellular neurexin-neuroligin interactions by enzymatic probe ligation. *PLoS One* **8,** e52823 (2013).

25. Pagliarini, D. J. *et al.* A Mitochondrial Protein Compendium Elucidates Complex I Disease Biology. *Cell* **134,** 112–123 (2008).

26. Richards, M. K. & Marletta, M. A. Characterization of Neuronal Nitric Oxide Synthase and a C415H Mutant, Purified from a Baculovirus Overexpression System. *Biochemistry* **33,** 14723–14732 (1994).

27. Martell, J. D. *et al.* Engineered ascorbate peroxidase as a genetically encoded reporter for electron microscopy. *Nat. Biotechnol.* **30,** 1143–8 (2012).

28. Kery, V., Elleder, D. & Kraus, J. P. Delta-aminolevulinate increases heme saturation and yield of human cystathionine beta-synthase expressed in Escherichia coli. *Arch. Biochem. Biophys.* **316,** 24–9 (1995).

29. Delcarte, J. *et al.* Optimisation of expression and immobilized metal ion affinity chromatographic purification of recombinant (His)6-tagged cytochrome P450 hydroperoxide lyase in Escherichia coli. *J. Chromatogr. B* **786,** 229–236 (2003).

30. Peroxidase, A., Barrows, T. P. & Poulos, T. L. Role of Electrostatics and Salt Bridges in Stabilizing the Compound I Radical in. 14062–14068 (2005).

31. Berry, E. A. & Trumpower, B. L. Simultaneous determination of hemes a, b, and c from pyridine hemochrome spectra. *Anal. Biochem.* **161,** 1–15 (1987).

32. Noble, R. W. & Gibson, Q. H. The Reaction of Ferrous Horseradish Peroxidase with Hydrogen Peroxide. *J. Biol. Chem.* **245,** 2409–2413 (1970).

33. Lad, L., Mewies, M. & Raven, E. L. Substrate Binding and Catalytic Mechanism in Ascorbate Peroxidase: Evidence for Two Ascorbate Binding Sites †. *Biochemistry* **41,** 13774–13781 (2002).